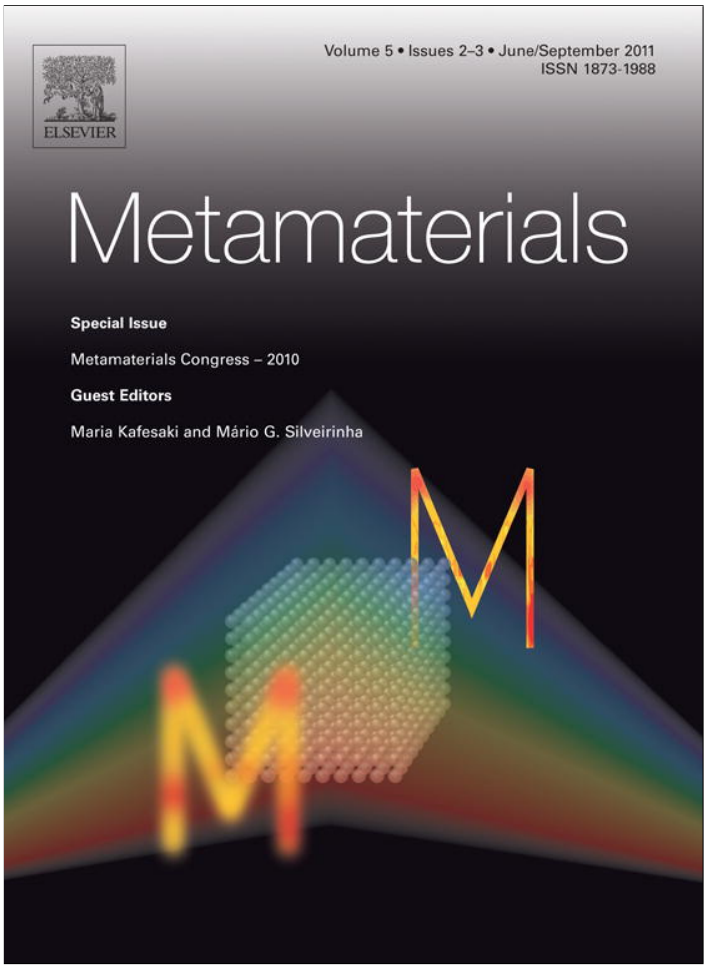

Available online at www.sciencedirect.com
ScienceDirect
Metamaterials 5 (2011) 112–118
Metamaterials
www.elsevier.com/locate/metmat

Super imaging with a plasmonic metamaterial: Role of aperture shape

Shiyi Xiao, Qiong He, Xueqing Huang, Lei Zhou *

State Key Laboratory of Surface Physics and Key Laboratory of Micro and Nano Photonic Structures (Ministry of Education), Fudan University, Shanghai 200433, China

Available online 14 April 2011

Abstract

Through analyzing the transmission properties of metallic plates with periodic arrays of subwavelength apertures in different shapes, we found two conditions for such structures to work as super lenses. The working wavelength dictated by the aperture's shape resonance should be much larger than the array's periodicity, meanwhile the coupling between the aperture's waveguide modes and external radiations should be as small as possible. These two conditions contradict with each other for a square-shape aperture so that high index materials should be inserted into the apertures, while a fractal-shape aperture satisfies these two conditions simultaneously without using high-index insertions. Numerical simulations were performed to illustrate the imaging properties of these plasmonic lenses.

Keywords: Metamaterials; Subwavelength imaging; Plasmonics

1. Introduction

Conventional optical imaging is subject to the diffraction limit so that the resolution is bounded by half of working wavelength. To realize subwavelength imaging demanded by many practical applications, an optical instrument should be able to collect information carried by both propagating and evanescent waves. In addition to conventional near-field optical approaches, many new ideas were recently proposed to achieve the super imaging. Realizing subwavelength imaging with metamaterials was first suggested by Pendry [1], who rigorously proved that a slab of material with $\varepsilon = \mu = -1$ is a perfect lens with infinitely high resolution, and the loss would degrade the resolution to make the lens a super one [2–4]. Although the idea was experimentally demonstrated in microwave regime [5,6], direct extension to higher frequencies is difficult since metamaterials with both ε and μ being -1 are hard to fabricate at optical frequencies. Relaxing the condition to let $\varepsilon = -1$ only, it was demonstrated that a silver slab could work as a super lens at a particular optical frequency, but only for near-field sources with specific polarization [7,8].

Subsequently, several new ideas to realize super imaging were proposed, which were still based on the metamaterial concept but did not require strictly $\varepsilon = \mu = -1$, and therefore, were more practically realizable. The proposed systems include layered metal-dielectric structures [9,10] and metallic wire media [11,12]. Although the working mechanisms are quite different, all these systems share a common characteristic that they can transfer the evanescent components from source to image planes without distortions. In addition, for these devices, the working wavelengths were typically determined by the geometrical structure instead of

* Corresponding author.
E-mail address: phzhou@fudan.edu.cn (L. Zhou).

1873-1988/$ – see front matter © 2011 Elsevier B.V. All rights reserved.
doi:10.1016/j.metmat.2011.03.005

constitutional material so that they can cover an ultra-wide frequency range upon structural design.

On the other hand, a new class of artificial materials, metallic plates with periodic array of apertures [13–20], drew a great deal of attention recently stimulated by the discovery of extraordinary optical transmission phenomenon [21]. In 2004, Pendry et al. demonstrated that metallic plates with slits or square holes support spoof surface plasmon polaritons (SPPs), and when the unit cells are enough subwavelength, such complex systems can be homogenized as plasmonic metamaterials with well-defined equivalent parameters. Inspired by these peculiar SPP properties, Jung et al. demonstrated by numerical simulations that a metallic plate with periodic slits could realize subwavelength imaging [22]. However, the image formed by such a super lens is subwavelength only along one direction (perpendicular to the slit), and the working wavelength is dependent of the lens thickness since a Fabry–Perot resonance is excited inside the slit [22]. To overcome these shortcomings, a metallic plate with fractal-like hole array was recently proposed as a super lens, and the imaging functionalities of the proposed devices were demonstrated by both numerical simulations and microwave experiments [23]. The image realized by the fractal lens is subwavelength along all directions and the working frequency is independent of the lens thickness [23].

There are, however, still several issues remaining unsolved. For example, the proposed fractal lens only works for sources with one particular polarization since the structure is inherently anisotropic [23]. Also, the role played by the aperture shape is not elucidated and it is not clear what happens if another shape is chosen. In this paper, we employ both theoretical analysis and finite-difference-time-domain (FDTD) simulations to address these issues. Through examining the transmission properties of such holey metallic plates (HMP) with different aperture shapes, we succeeded in identifying two important conditions to ensure these structures working as super lenses. These conditions would guide people search for structures with good imaging performances and help understand the intrinsic mechanisms underlying the super imaging effect.

2. Theoretical analysis

Suppose a y-polarized dipole source, taking the simplest current distribution as $\vec{J}(\vec{r}, t) = \hat{y} P_0 \delta(\vec{r}) e^{-i\omega t}$ with P_0 and $\delta(\vec{r})$ defining the strength and position of the dipole source, is put on top of a slab lens as shown in Fig. 1(a). The electromagnetic (EM) field distribution can be formally solved using a dyadic Green's function

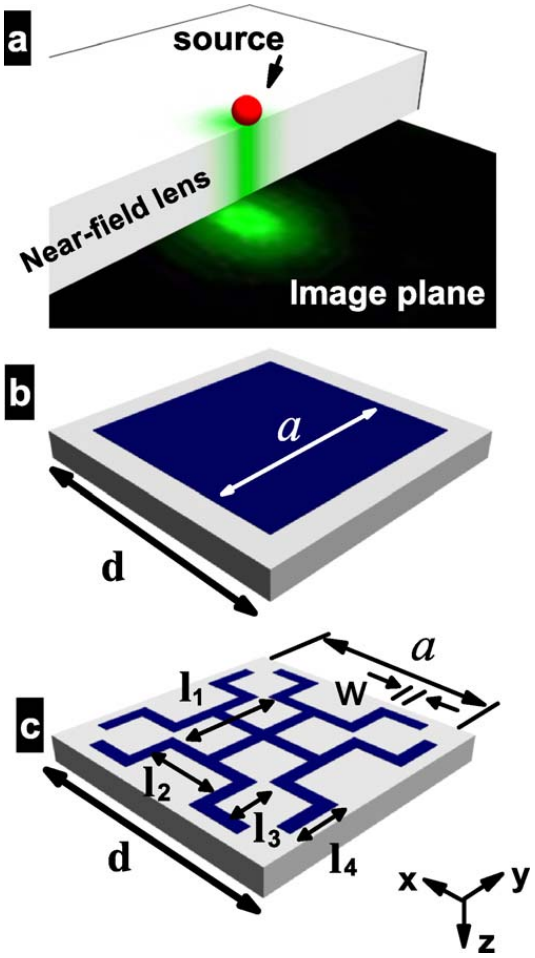

Fig. 1. (a) Geometry of the near-field super imaging. Unit cell structures of holey metallic plates with (b) square holes and (c) fractal-like slit patterns.

method, based on decoupling the radiation fields into a series of plane waves with different incident angles and polarizations [24,25]. For example, on the image plane which is the exit surface of the slab lens, the y component of E-field is found explicitly as:

$$E_y(x, y) = -\frac{i\mu_0 P_0}{8\pi^2} \int \frac{e^{ik_\parallel (x\cos\phi + y\sin\phi)}}{k_z} \times \left[T^{\mathrm{TE}}(k_\parallel)\cos^2\phi + \frac{k_z^2}{k_0^2} T^{\mathrm{TM}}(k_\parallel)\sin^2\phi \right] k_\parallel dk_\parallel \, d\phi \quad (1)$$

where $k_z = \sqrt{k_0^2 - k_\parallel^2}$ with $k_0 = \omega/c$, ϕ is the azimuth angle, $T^{\mathrm{TE}}(k_\parallel)$ and $T^{\mathrm{TM}}(k_\parallel)$ are the transfer functions of the slab lens for incident plane waves in transverse-electric (TE) and transverse-magnetic (TM) polarizations and with a particular parallel $\mathbf{k}$ component. Here we suppose the lens is isotropic on the x–y plane.

We immediately find that the transmission properties of the slab are essential for the imaging performance.

If at some frequencies the slab is designed to exhibit $T^{\mathrm{TE}}(k_\parallel) \equiv 1$ and $T^{\mathrm{TM}}(k_\parallel) \equiv 1$ for all $k_\parallel$ values (no matter $k_\parallel < k_0$ for propagating component or $k_\parallel > k_0$ for evanescent component), Eq. (1) tells us that the field distribution on the image plane is *identical* to that on the source plane so that the slab lens is a *perfect* one.[1] The physics is that such a lens can *perfectly* transfer all Fourier wave-components through it without any distortion.

We now analyze the transmission properties of a HMP. The shape of the aperture can be a simple square [see Fig. 1(b)] or other complex geometry [Fig. 1(c)], but it should exhibit the 4-fold symmetry on the x–y plane. Without losing generality, we assume that each aperture is filled with certain dielectric medium with dielectric constant ε_h. Such a problem is analytically solvable under some approximations. Suppose a plane wave with certain polarization and parallel **k** vector is incident from air on the HMP, the wave transmitted through the structure can be solved using the mode-expansion technique developed in Refs. [24,25]. Retaining only the fundamental scattering mode in air regions and the fundamental waveguide mode inside the holes, we solved the scattering problem analytically by appropriately matching the boundary conditions. Extending the previously established mode-expansion technique for simple square shape [13,22] to arbitrary *symmetrical* shape, we obtained the transmission/reflection coefficients through a finite-thickness HMP. Explicitly, the transmission coefficients were found as:

$$\begin{aligned} T^{\mathrm{TE}}(k_\parallel) &= \frac{4Y_0^{\mathrm{TE}} Y_{\mathrm{hole}} e^{iq_z h}}{(Y_0^{\mathrm{TE}} + Y_{\mathrm{hole}})^2 - (Y_0^{\mathrm{TE}} - Y_{\mathrm{hole}})^2 e^{2iq_z h}} \\ T^{\mathrm{TM}}(k_\parallel) &= \frac{4Y_0^{\mathrm{TM}} Y_{\mathrm{hole}} e^{iq_z h}}{(Y_0^{\mathrm{TM}} + Y_{\mathrm{hole}})^2 - (Y_0^{\mathrm{TM}} - Y_{\mathrm{hole}})^2 e^{2iq_z h}} \end{aligned} \tag{2}$$

where $Y_{\mathrm{hole}} = q_z / S_0^2 \omega\mu_0$ is the admittance of the fundamental waveguide mode within the holes and $q_z = k_0 \cdot \sqrt{\varepsilon_h} \cdot \sqrt{1 - \omega_c^2/\omega^2}$ with ω_c being the cutoff frequency of the waveguide,[2] $Y_0^{\mathrm{TE}} = k_z/\omega\mu_0$ and $Y_0^{\mathrm{TM}} = \omega\varepsilon_0/k_z$ are the admittance of the scattering wave in air where $k_z = \sqrt{k_0^2 - k_\parallel^2}$, and S_0 is the overlapping integral between incident plane wave and the fundamental waveguide mode, representing the strength of coupling between them. For normal incidence case, S_0 is found as

$$S_0 = \frac{\int_{\mathrm{hole}} E_y^{\mathrm{Inc}*} \cdot E_y^{\mathrm{WG}} dx\, dy}{\int_{\mathrm{hole}} (|E_x^{\mathrm{WG}}|^2 + |E_y^{\mathrm{WG}}|^2) \cdot dx\, dy}, \tag{3}$$

where the integration is taken over the hole area, $\vec{E}^{\mathrm{Inc}}$ is the incident plane wave with polarization $\vec{E}^{\mathrm{Inc}} \| \hat{y}$, and $\vec{E}^{\mathrm{WG}}$ denotes the field pattern of the fundamental waveguide mode, which can be obtained by numerical simulations. In the simplest case of square shape [Fig. 1(b)], we found analytically that:

$$S_0 = \frac{2\sqrt{2}a}{\pi d} \tag{4}$$

which coincides with an early analytical result [13,22].

An important conclusion can be drawn by analyzing Eq. (2). As $\omega \to \omega_c$ so that $q_z \to 0$, we can expand the transmission coefficients to power series of q_z. Keeping the lowest-order terms in q_z, we found that

$$\begin{cases} T^{\mathrm{TE}}(k_\parallel) = \dfrac{1}{[1 - (S_0^2/2)(2\pi h/\lambda)i] + O(q_z)} \\ T^{\mathrm{TM}}(k_\parallel) = \dfrac{1}{[1 - (S_0^2/2)(2\pi h/\lambda)i] + O(q_z)} \end{cases} \tag{5}$$

Eq. (5) is remarkable, since it predicts that

$$T^{\mathrm{TE}}(k_\parallel), \quad T^{\mathrm{TM}}(k_\parallel) \to 1 \tag{6}$$

for all values of $k_\parallel$, if the condition

$$S_0 \ll 1 \tag{7}$$

is satisfied. Therefore, put Eq. (6) to Eq. (1), we found that the system behaves as a *perfect* lens at the frequency $\omega = \omega_c$. In addition, for this particular case, the working frequency is solely dependent on the lateral geometry of the aperture and has nothing to do with the thickness h of the HMP. Therefore, in principle one can make a thick HMP to transmit a perfect image through a very long distance.

However, we have to mention that Eqs. (2) and (5) are obtained under two important assumptions – the higher order diffractions in air regions and the higher-order modes in waveguides can be neglected. The first assumption is easily justified if we have

$$\lambda_c \gg d \tag{8}$$

so that all higher order diffraction modes are evanescent waves. We will demonstrate in Sec. III that the second assumption is justified if the condition (7) is satisfied.

[1] We note that E_y distribution on the source plane can expressed as: $E_y(x, y) = -\frac{i\mu_0 P_0}{8\pi^2} \int (e^{ik_\parallel (x\cos\phi + y\sin\phi)}/k_{0z})[(1 + R^{\mathrm{TE}}(k_\parallel))\cos^2\phi + (k_{0z}^2/k^2)(1 - R^{\mathrm{TM}}(k_\parallel))\sin^2\phi] k_\parallel dk_\parallel d\phi$. Therefore, when the condition $T^{\mathrm{TE}}(k_\parallel) \equiv 1$, $T^{\mathrm{TM}}(k_\parallel) \equiv 1$ (indicating $R^{\mathrm{TE}}(k_\parallel)$, $R^{\mathrm{TM}}(k_\parallel) \equiv 0$ simultaneously) is satisfied, we find that the field distribution on the image plane (Eq. (1)) is identical to that on the source plane.

[2] For a square shape, the fundamental waveguide mode is just the TE_{10} mode and $\omega_c = c\pi/(a\sqrt{\varepsilon_h})$. For arbitrary symmetrical shape, the fundamental mode information can be obtained by numerical simulations.

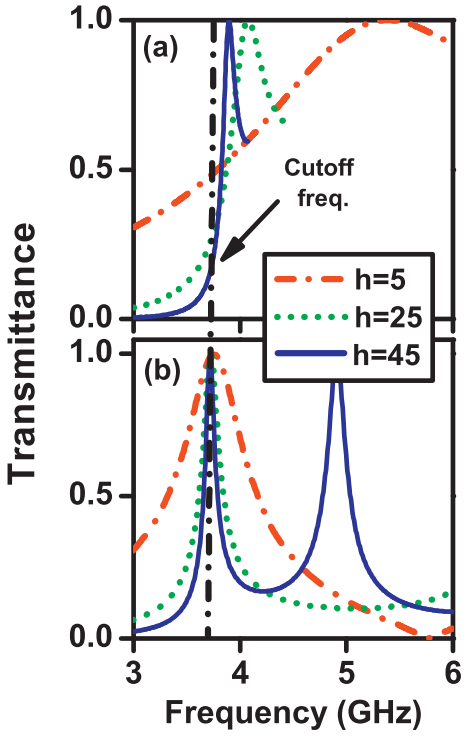

Fig. 2. FDTD calculated transmission spectra for a series of (a) square-aperture and (b) fractal-aperture HMPs with different thickness h and with $a = 18$ mm. The cutoff frequency is 3.75 GHz for both apertures (dashed line). The geometrical parameters of the fractal pattern are $d = 20$ mm, $l_1 = 12$ mm, $l_2 = 8$ mm, $l_3 = l_4 = 4$ mm, and $w = 1$ mm.

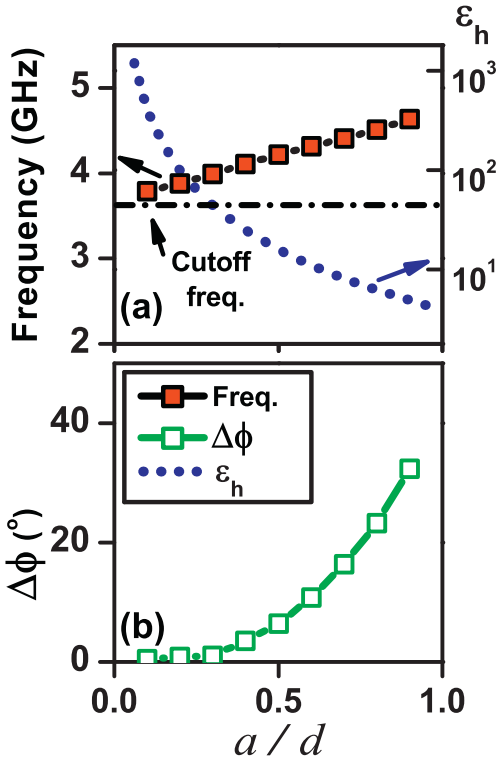

Fig. 3. (a) Perfect transmission frequencies (squares) and (b) the associated phase changes $\Delta\phi$ for square-aperture HMPs with different values of a/d, calculated by FDTD simulations. Here the thicknesses of the HMPs are fixed as $h = 10$ mm. Dotted line depicts the permittivity ε_h of the inserting materials in order to keep the cutoff frequency of the systems fixed as 3.75 GHz.

3. Numerical analyses on realistic structures

In this section, we take the square-shape aperture [Fig. 1(b)] as an example to identify the criterion for the second assumption. In all the structures (with either square or fractal apertures) studied in this paper, we fixed the periodicity as $d = 20$ mm. We first employed FDTD simulations[3] to calculate the normal-incidence transmission spectra through a series of HMPs with a fixed as $a/d = 0.9$ but with different thickness h, and depicted the spectra in Fig. 2(a). Here we set $\varepsilon_h = 400/81$ so that the cutoff wavelength is $\lambda_c = 4_d$, satisfying the condition (8). We found that perfect transmission frequencies for these HMPs are not precisely ω_c, but rather strongly depend on the thickness h. This is in direct contradiction with Eq. (6) which predicts that perfect transmission always occurs at the cutoff frequency ω_c. Apparently, the single-mode approximation is not valid here.

We then varied the value of a/d to see what kind of aperture would better support the single-mode approximation. To ensure each waveguide to exhibit the same cutoff wavelength $\lambda_c = 4_d$, we purposely set $\varepsilon_h = 4 \times (d/a)^2$ for each HMP. We employed FDTD simulations to study the transmission spectra of these HMPs (with h fixed as 10 mm), and depicted in Fig. 3(a) and (b) the perfect transmission frequency and the transmission phase as functions of a/d, respectively. Clearly, only in the limit of $a/d \to 0$, perfect transmission occurs at the cutoff frequency and the associated phase change $\Delta\phi \to 0$, in consistency with Eq. (6) obtained under the single-mode approximation. Therefore, the value of a/d is a crucial criterion to justify the single-mode assumption. Noting that the overlapping strength S_0 is proportional to a/d in the square-shape aperture case [see Eq. (4)], we conclude that Eq. (7) is just the criterion to validate the single-mode assumption inside the waveguide. In fact, criterion Eq. (7) has a profound physical significance, since S_0 actually measures the quality (Q) factor of the aperture resonator. Indeed, for an aperture with a higher Q-factor, the single-mode approximation is better applicable since the external radiation can only excite this particular mode.

To visualize the super imaging effects, we performed FDTD simulations to study the images formed by four square-aperture HMPs with different values of a/d, and

[3] CONCERTO 7.0, Vector Fields Limited, England (2008).

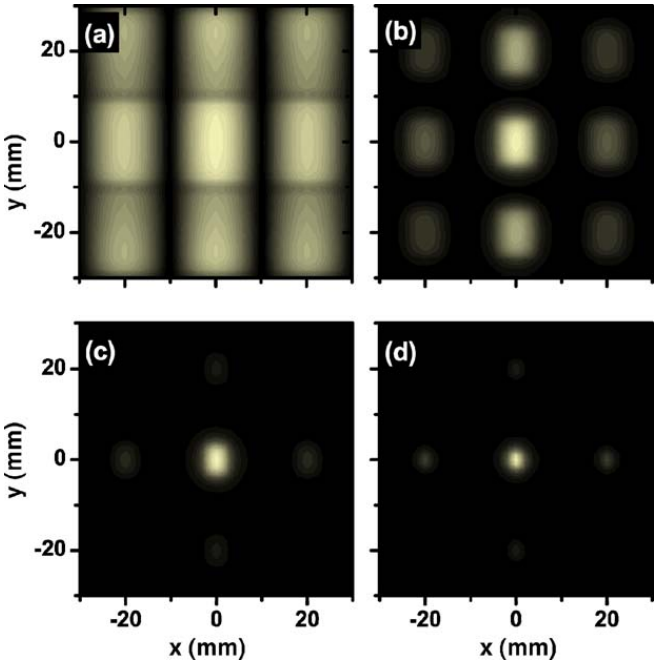

Fig. 4. FDTD calculated *E*-field patterns on the image planes of four square-aperture HMPs with different values of *a*/*d*: (a) $a/d = 0.9$, (b) $a/d = 0.5$, (c) $a/d = 0.3$ and (d) $a/d = 0.1$. In all cases, a dipole source polarized along *y* axis is put at the origin point on the source plane and the working frequency is 3.75 GHz.

depicted the calculated patterns in Fig. 4(a–d). All these HMPs are designed to have the same thickness $h = 5$ mm and cutoff frequency 3.75 GHz through adjusting the value of ε_h. In the case of large *a*/*d*, we found that the formed image is very bad without any feature [Fig. 4(a)]. However, the image quality becomes better and better as *a*/*d* decreases [see Fig. 4(b–d)], which justifies our arguments presented above.

Eqs. (7) and (8) are two analytical conditions for an HMP to work as a super lens. For an HMP with square-shape apertures, these two conditions can only be satisfied when the aperture is filled with high-index materials. As shown by the dotted line in Fig. 3(a), ε_h should increase to a very large value (over 1000) to make the single-mode approximation applicable. However, material with such a high ε_h is not easy to find in practice. Fortunately, we found that these two conditions can be simultaneously satisfied for other shapes including the fractal pattern, without using any high-index insertion. The physics is that a fractal pattern could sustain a cutoff wavelength much longer than its own lateral size.

We note that the previously designed fractal lens only works for sources with a fixed *E*-field polarization [23], since the fractal pattern itself is anisotropic. Here we extended the previous idea [23] to design an *isotropic* fractal-like HMP with unit cell shown in Fig. 1(c), and studied its imaging functionalities. Set the lateral size

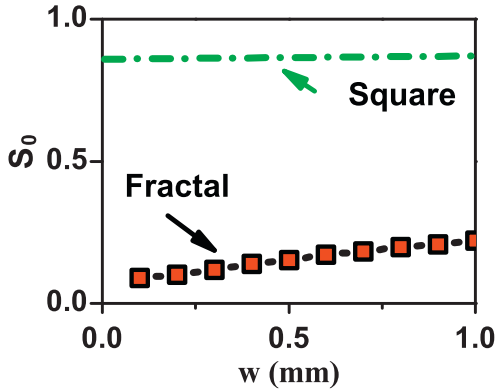

Fig. 5. S_0 of the fractal aperture as a function of slit line width *w*, calculated by FDTD simulations. The dashed line denotes the value of S_0 for a square aperture. Both apertures have $a/d = 0.9$.

of the fractal pattern is the same of that of the square aperture, i.e., $a/d = 0.9$, we first employed FDTD simulations to study the transmission spectra through a series of HMPs with different thicknesses *h*, and compared the results in Fig. 2(b). In sharp contrast to Fig. 2(a) for the square-aperture HMP with the same *a*/*d* value, here for the fractal-aperture case the perfect transmission frequency is robust against *h*, indicating that the transmission phase is nearly zero and the single-mode approximation [and its prediction Eq. (6)] is valid.

To understand why the fractal-aperture lens is more superior than the square-aperture lens, we employed FDTD simulations to numerically compute the overlapping strength S_0 based on Eq. (3) for the fractal aperture. Calculations show that, in contrast to the square-aperture case where S_0 is solely determined by *a*/*d*, here for a fractal shape S_0 can be tuned by an additional parameter – the width *w* of each slit. As shown in Fig. 5 where S_0 is depicted as a function of *w*, we find that S_0 of the fractal aperture can be made much smaller than that of the square aperture (both have $a/d = 0.9$) by simply decreasing *w*. This explains why the single-mode assumption works so well for the fractal HMP, simply because the condition (7) can be better satisfied by narrowing the line width *w* so as to increase the *Q*-factor.

As an illustration, we employed FDTD simulations to study the transfer functions [$T^{\mathrm{TE}}(k_\parallel)$ and $T^{\mathrm{TM}}(k_\parallel)$] for the designed isotropic fractal-like HMP. The results depicted in Fig. 6 verified that indeed we have $T^{\mathrm{TM}}(k_\parallel)$, $T^{\mathrm{TE}}(k_\parallel) \approx 1$ for both transmission amplitudes and phases, at the working frequency 3.75 GHz. The inherent reason is that our structure supports TE and TM polarized spoof SPPs simultaneously, which has been demonstrated in our previous work [23]. We further employed FDTD simulations to compute the image formed by such a lens for a point source polarized

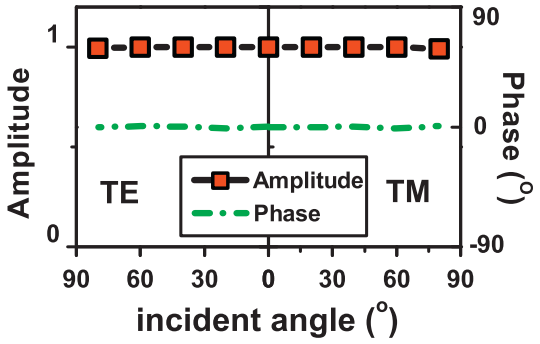

Fig. 6. Amplitude (squares, left axis) and $\Delta\phi$ (dashed line, right axis) of the transfer functions T^{TE} and T^{TM} of a fractal-aperture HMP with $h = 5$ mm, as functions of incident angles calculated by FDTD simulations at 3.75 GHz.

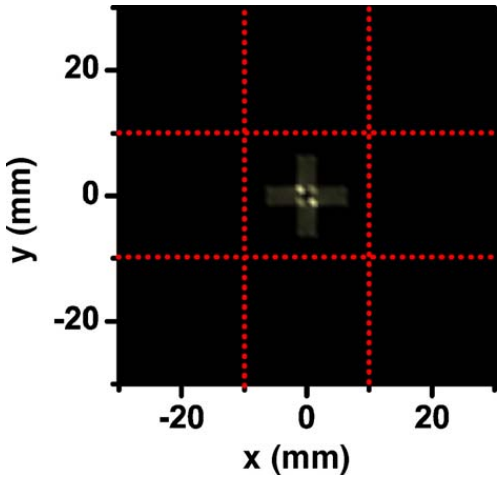

Fig. 7. FDTD calculated E-field pattern on the image plane of a 5-mm thick fractal-aperture HMP, with a dipole source polarized along $-\hat{x} + \hat{y}$ direction put at the origin point of the source plane.

along $-\hat{x} + \hat{y}$ direction, and the image pattern depicted in Fig. 7 indeed resembles a dipole polarized along 135°, although two additional weak bright-spots appear in the image plane caused by scatterings on the aperture corners. Fig. 7 demonstrates that the system is a two-dimensionally *isotropic super* lens with much better imaging quality compared to the square-shape HMP with the same *a/d* [Fig. 4(a)]. Most importantly, here for the fractal lens no high-index material is needed to achieve the super imaging effect.

Finally, we emphasize that it is inappropriate to derive the image resolutions directly from the patterns shown in Figs. 4 and 7, since the resolution is ultimately bounded the lattice constant d of the HMP [23]. However, a better field confinement within a unit cell (such as the cases shown in Figs. 4 and 7(c–d)) is still extremely helpful for the super lens to achieve the desired limiting resolution.

4. Conclusions

In short, through analyzing the transmission properties of HMPs with apertures in different shapes, we found two analytical conditions for such systems to work as super lenses. We employed FDTD simulations to study the imaging functionalities of two types of super lenses, and found that the aperture shape plays a crucial role in achieving the super imaging effect.

Acknowledgements

This work was supported by the National Natural Science Foundation of China (Nos. 60725417, 60990321), Shanghai Science and Technology Committee (08dj1400302), and MOE of China (B06011).

References

[1] J.B. Pendry, Negative refraction makes a perfect lens, Phys. Rev. Lett. 85 (2000) 3966.
[2] J.B. Pendry, Comment on 'Left-handed materials do not make a perfect lens', Phys. Rev. Lett. 91 (2003) 099701.
[3] D.O.S. Melville, Richard J. Blaikie, Conrad R. Wolf, Submicron imaging with a planar silver lens, Appl. Phys. Lett. 84 (2004) 4403.
[4] D.R. Smith, D. Schurig, J.B. Pendry, Negative refraction of modulated electromagnetic waves, Appl. Phys. Lett. 81 (2002) 2713.
[5] A. Grbic, G.V. Eleftheriades, Overcoming the diffraction limit with a planar left-handed transmission-line lens, Phys. Rev. Lett. 92 (2004) 117403.
[6] A.N. Lagarkov, V.N. Kissel, Near-perfect imaging in a focusing system based on a left-handed-material plate, Phys. Rev. Lett. 92 (2004) 077401.
[7] N. Fang, H. Lee, C. Sun, X. Zhang, Sub-diffraction-limited optical imaging with a silver superlens, Science 308 (2005) 534.
[8] D.O.S. Melville, R.J. Blaikie, Super-resolution imaging through a planar silver layer, Opt. Express 13 (6) (2005) 2127.
[9] S.A. Ramakrishna, J.B. Pendry, M.C.K. Wiltshire, W.J. Stewart, Imaging the near-field, J. Mod. Opt. 50 (2003) 1419.
[10] P.A. Belov, Y. Hao, Subwavelength imaging at optical frequencies using a transmission device formed by a periodic layered metal-dielectric structure operating in the canalization regime, Phys. Rev. B 73 (2006) 113110.
[11] P.A. Belov, Y. Hao, S. Sudhakaran, Subwavelength microwave imaging using an array of parallel conducting wires as a lens, Phys. Rev. B 73 (2006) 033108.
[12] G. Shvets, S. Trendafilov, J.B. Pendry, A. Sarychev, Guiding, focusing, and sensing on the subwavelength scale using metallic wire arrays, Phys. Rev. Lett. 99 (2007) 053903.
[13] F.J. Garcia-Vidal, L. Martin-Moreno, J.B. Pendry, Surface with holes in them: new plasmonic metamaterials, J. Opt. A: Pure Appl. Opt. 7 (2005) S97.
[14] J.B. Pendry, L. Martin-Moreno, F.J. Garcia-Vidal, Mimicking surface plasmons with structured surfaces, Science 305 (2004) 847.

[15] F.J. Garcia-Vidal, L. Martin-Moreno, T.W. Ebbesen, L. Kuipers, Light passing through subwavelength apertures, Rev. Mod. Phys. 82 (2010) 729–787.
[16] M. Beruete, M. Sorolla, I. Campillo, J.S. Dolado, L. Martín-Moreno, J. Bravo-Abad, F.J. García-Vidal, Enhanced millimeter-wave transmission through subwavelength hole arrays, Opt. Lett. 29 (2004) 2500–2502.
[17] A. Ishimaru, Electromagnetic Wave Propagation, Radiation and Scattering, Prentice-Hall, Englewood Cliffs, NJ, 1991.
[18] A.A. Oliner, D.R. Jackson, Leaky surface-plasmon theory for dramatically enhanced transmission through a subwavelength aperture, part I: basic features, in: Proc. IEEE AP-S Symp. Radio Sci., vol. 2, 2003, pp. 1091–1094.
[19] D.R. Jackson, T. Zhao, J.T. Williams, A.A. Oliner, Leaky surface-plasmon theory for dramatically enhanced transmission through a sub-wavelength aperture, part II: leaky-wave antenna model, in: Proc. IEEE AP-S Symp. Radio Sci., vol. 2, 2003, pp. 1095–1098.
[20] C. Lertsirimit, D.R. Jackson, D.R. Wilton, Time-domain coupling to a device on printed circuit board inside a cavity, Radio Sci. 40 (2005) 1–12.
[21] T.W. Ebbesen, H.J. Lezec, H.F. Ghaemi, T. Thio, P.A. Wolff, Extraordinary optical transmission through sub-wavelength hole arrays, Nature 391 (1998) 667–669.
[22] J. Jung, F.J. García-Vidal, L. Martín-Moreno, J.B. Pendry, Holey metal films make perfect endoscopes, Phys. Rev. B 79 (2009) 153407.
[23] X. Huang, S. Xiao, D. Ye, J. Huangfu, Z. Wang, L. Ran, L. Zhou, Fractal plasmonic metamaterials for subwavelength imaging, Opt. Express 18 (2010) 10377.
[24] L. Zhou, C.T. Chan, Relaxation mechanisms in three-dimensional metamaterial lens focusing, Opt. Lett. 30 (2005) 1812.
[25] L. Zhou, X. Huang, C.T. Chan, A time-dependent Green's function approach to study the transient phenomena in metamaterial lens focusing, Photon. Nanostruct.: Fundam. Appl. 3 (2005) 100.